Hysteresis-Free Negative Capacitance Effect in Metal-Ferroelectric-Insulator-Metal Capacitors with Dielectric Leakage and Interfacial Trapped Charges

Chia-Sheng Hsu,[1,*] Sou-Chi Chang,[2] Dmitri E. Nikonov,[2] Ian A. Young,[2] and Azad Naeemi[1]

[1] *School of Electrical and Computer Engineering, Georgia Institute of Technology, Atlanta, Georgia 30332, USA*

[2] *Components Research, Intel Corporation, Hillsboro, Oregon 97124, USA*

(Received 4 December 2020; revised 18 February 2021; accepted 26 February 2021; published 16 March 2021)

The negative capacitance (NC) stabilization of a ferroelectric (FE) material can potentially provide an alternative way to further reduce the power consumption in ultrascaled devices and thus has been of great interest in technology and science in the past decade. In this paper, we present a physical picture for a better understanding of the hysteresis-free charge-boost effect observed experimentally in metal-ferroelectric-insulator-metal (*M*-*F*-*I*-*M*) capacitors. By introducing the dielectric (DE) leakage and interfacial trapped charges, our simulations of the hysteresis loops are in a strong agreement with the experimental measurements, suggesting the existence of an interfacial oxide layer at the FE-metal interface in metal-ferroelectric-metal (*M*-*F*-*M*) capacitors. Based on the pulse-switching measurements, we find that the charge enhancement and hysteresis are dominated by the FE domain viscosity and DE leakage, respectively. Our simulation results show that the underlying mechanisms for the observed hysteresis-free charge enhancement in *M*-*F*-*I*-*M* may be physically different from the alleged NC stabilization and capacitance matching. Moreover, the link between Merz's law and the phenomenological kinetic coefficient is discussed, and the possible cause of the residual charges observed after pulse switching is explained by the trapped charge dynamics at the FE-DE interface. The physical interpretation presented in this work can provide useful insights into the NC effect in *M*-*F*-*I*-*M* capacitors and future studies of low-power logic devices.

DOI: 10.1103/PhysRevApplied.15.034048

I. INTRODUCTION

As the relentless pursuit of device miniaturization goes into the nanometer regime, Moore's law has gradually come to a bottleneck due to the fact that the power dissipation in microchips becomes a more and more challenging concern [1,2]. Recently, a stack structure consisting of a ferroelectric (FE) layer and a dielectric (DE) layer was proposed to achieve voltage amplification in a DE layer [3]. The physical concept behind this approach is that the metastable negative capacitance (NC) state arising from the double-well energy profile of the FE can be stabilized by the DE layer in terms of the total free energy of the system. Such a proposal may provide a potential way to significantly improve the subthreshold swing of conventional CMOS transistors at room temperature [4,5].

Ferroelectrics are materials that exhibit the properties: (i) the electric polarization can be reversed by an externally applied voltage and (ii) the remanent polarization remains nonvolatile under zero bias. These unique properties have made ferroelectrics promising materials for voltage-controlled nonvolatile memory devices [6,7]. In the past decade since the proposal of using NC for low-power logic devices, FE-based capacitors, including metal-ferroelectric-metal (*M*-*F*-*M*), metal-ferroelectric-insulator-metal (*M*-*F*-*I*-*M*), and metal-ferroelectric-metal-insulator-metal (*M*-*F*-*M*-*I*-*M*), have been intensively investigated experimentally and theoretically in search of the evidence for the transient and steady-state NC effects [8–17]. In particular, recently discovered doped hafnium oxides are widely used as the FE layer due to the high scalability and CMOS process compatibility [18–20].

With a *M*-*F*-*M* capacitor connected in series with a large resistor, the transient NC behaviors have been observed in various FE materials, including perovskite $Pb(Zr_{0.2}Ti_{0.8})O_3$ and various doped hafnium oxides [8,12,21]. The physical origin of the observed transient NC lies in the mismatch between the switching rates of free charges and bound charges (FE polarization) in the resistor-capacitor circuit [13]. To further seek the evidence of static NC stabilization, FE-DE stacks are the key devices to be investigated according to the NC theory. Among *M*-*F*-*I*-*M*, *M*-*F*-*M*-*I*-*M*, and FE-DE superlattices, *M*-*F*-*I*-*M* capacitors are extremely useful because of the

*chiasheng@gatech.edu

 © 2021 American Physical Society

structure similarity to ferroelectric FETs (FEFETs). For M-F-I-M stacks, it is unlikely to directly measure the internal DE voltage amplification, which was theoretically proposed to be achieved by the steady-state NC stabilization. Therefore, a considerable amount of experimental efforts have been focused on the evidence of capacitance enhancement in a M-F-I-M capacitor compared to the associated standalone DE capacitor [22]. Such a capacitance enhancement is referred to as the charge-boost effect.

In the recent research progress, it was experimentally observed that the charge-boost effect and hysteresis-free static "S-shaped curve" could be achieved in M-F-I-M with short pulse measurements [14,15]. On one hand, the charge boost may indicate that the M-F-I-M capacitor has a larger capacitance than the associated DE capacitor, which was allegedly caused by the NC stabilization. On the other hand, the observed hysteresis-free FE switching (S curve), which is predicted by the Landau phenomenological formalism, is a required characteristic for the logic applications. However, the physical mechanisms for these observations are still not clear. For example, Liu *et al.* have recently proposed an alternative perspective on such experimental observations [23]. Therefore, it is beneficial to further explore the underlying physical mechanisms for such prospective experimental evidence of NC stabilization.

In this paper, we establish a physical model for M-F-M and M-F-I-M capacitors by introducing the inevitable DE leakage and trapped charges at the FE-DE interface. We show that the experimentally measured hysteresis loop of M-F-M capacitors can be well described by the Landau formalism with the proposed physical mechanisms included. The charge-boost and hysteresis behaviors observed in the pulse measurements are found to be directly influenced by the FE intrinsic domain viscosity and DE leakage, respectively. The kinetic coefficients extracted from the charge responses are found to be linked to the well-known Merz's law [24] in the NC region. Our simulation results suggest that the experimentally observed hysteresis-free capacitance enhancement of M-F-I-M may be caused not by the NC stabilization and capacitance matching but by the material properties of the heterostructure. Furthermore, the possible cause of the experimentally observed residual charges may be explained by the trapped charges existing at the FE-DE interface.

This paper is organized as follows. In Sec. II, the theoretical approach is presented to describe the switching characteristics of M-F-M and M-F-I-M capacitors, with the DE leakage and trapped charge mechanisms included. In Sec. III, based on the physical model, the FE material parameters can be well extracted using the hysteresis measurements. Significantly, the experimentally observed charge boost and hysteresis-free static S curve are well captured, and a physical picture for such phenomena is provided and discussed in detail. In Sec. IV, we conclude this work by highlighting the underlying mechanisms for experimental observations.

II. THEORETICAL FORMALISM

To describe the electrical properties of M-F-I-M bilayer stacks measured in the experiments, Kirchhoff's law is applied for the schematic circuit diagram shown in Fig. 1. The total current I_R flowing through the series resistor is thus expressed as

$$I_R = A\frac{\partial Q_f}{\partial t} = \frac{V_{\text{in}} - V_{\text{out}}}{R}, \tag{1}$$

where Q_f is the free charge density, R is the series resistance, and A is the capacitor area. In addition, the following conditions have to be satisfied by assuming the electric displacement field is continuous at material boundaries:

$$I_R = I_{\text{FE}} = I_{\text{DE}} + I_L, \tag{2}$$

where I_L represents the DE leakage current, and I_{FE} and I_{DE} are the displacement current of the FE and the DE layers, respectively. Instead of the conventional dc leakage current, I_L here describes the transient DE leakage due to the voltage across the DE layer, as is detailed later.

In the FE layer, the displacement charge density Q_{FE} can be written as

$$Q_{\text{FE}} = \epsilon_0 \kappa E_{\text{FE}} + P, \tag{3}$$

where ϵ_0 is the vacuum dielectric constant, κ is the background dielectric constant of the FE material [25], E_{FE} is the electric field across the FE oxide, and P is the average FE polarization. The dynamics of P is governed by the

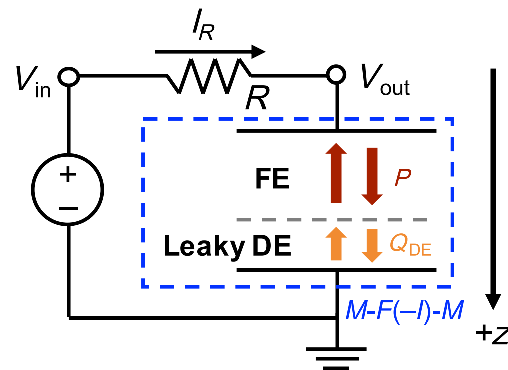

FIG. 1. Schematic diagram of a resistor-capacitor circuit for the study of switching dynamics in the experimental measurements. The positive axis is defined as the z direction toward ground.

Landau-Khalatnikov (LK) equation,

$$\frac{\partial P}{\partial t} = -L(2\alpha_1 P + 4\alpha_{11}P^3 + 6\alpha_{111}P^5 - E_{\mathrm{FE}}), \quad (4)$$

where $\{\alpha_1, \alpha_{11}, \alpha_{111}\}$ are thermodynamic expansion coefficients for the bulk FE free energy, and L is the kinetic coefficient, which is inversely proportional to domain viscosity [5,13,26–28]. Note that with the kinetic coefficient that can capture the multidomain nature of the FE, Eq. (4) is used as an approximation that describes the macroscopic polarization dynamics without considering the polarization gradient and the corresponding domain interactions in polycrystalline films [17,29]. In general, the leakage of a HfO_2-based FE may depend on the doping element, the doping ratio as well as the electrode materials [12,30]. Previous experimental studies have found that the leakage of $Hf_{0.5}Zr_{0.5}O_2$ (HZO) capacitors with tungsten nitride metal contacts does not significantly increase until the FE thickness is scaled down to 4 nm and below [30]. Moreover, further analyses based on the experimental measurements in Refs. [12] and [14] also show that the leakage of the 11.3-nm FE HZO is negligible for the *M-F-M* and *M-F-I-M* capacitors in this study. As a result, the free charge density Q_f is equal to the FE displacement charge density Q_{FE}.

It was experimentally reported that the trapped charges may exist at the FE-DE interface through the DE leakage, which plays a role in the electrical properties and DE breakdown of *M-F-I-M* capacitors [31]. In this regard, we introduce DE leakage and interfacial trapped charges into the *M-F-M* and *M-F-I-M* systems. According to the experiments on ultrathin Al_2O_3 (AO) dielectrics [32], the DE leakage approximated as field-assisted tunneling can be generally expressed as

$$I_L = \mathrm{sgn}(E_{\mathrm{DE}})\alpha E_{\mathrm{DE}}^2 \exp(-\beta/|E_{\mathrm{DE}}|) \times A, \quad (5)$$

where E_{DE} is the electric field across the DE oxide, α and β are physical parameters determined by the electron effective mass and the tunneling barrier height, and a sign function is used for the current direction. The leakage current when the DE voltage V_{DE} is below a cutoff voltage V_c is assumed to be negligible for simplicity, where V_c is set to 0.2 V in this work. Extracted from the experimental measurements in Ref. [14], β in Eq. (5) is found to be a small constant value of 3.7×10^{-7} V/m for all the simulations. Note that the leakage current level obtained from the experiments is much smaller than that predicted by conventional Fowler-Nordheim (FN) tunneling, where α and β are not independent of each other. The smaller transient leakage current measured in the experiments may possibly be attributed to the charges temporarily trapped in the DE layer during the tunneling process, whereas FN tunneling formalism captures a much larger leakage current in the steady state, where more charges can tunnel through the DE layer. Therefore, the transient leakage current may depend on charge trapping inside the DE layer, and may not be directly described by conventional FN tunneling.

To extract the DE charge density (Q_{DE}) accumulated at the DE-metal interface, we integrate the displacement current through the DE layer with respect to time:

$$Q_{\mathrm{DE}}(t) = \frac{1}{A}\int_0^t I_{\mathrm{DE}}(\tau)d\tau + Q_{\mathrm{DE}}(0), \quad (6)$$

where $Q_{\mathrm{DE}}(0)$ is the DE charges before switching. Note that $Q_{\mathrm{DE}}(0)$ is an initial condition in this framework and may vary from sample to sample depending on the experimental conditions.

At the FD-DE interface, the charge neutrality condition has to be satisfied due to the displacement field continuity in the normal direction. Therefore, the interfacial trapped charge Q_{it} can be obtained with the expression given by

$$Q_{\mathrm{FE}} + \widetilde{Q}_{\mathrm{DE}} + Q_{\mathrm{it}} = 0, \quad (7)$$

where $\widetilde{Q}_{\mathrm{DE}} = -Q_{\mathrm{DE}}$ is the DE charge at the FE-DE interface.

III. RESULTS AND DISCUSSION

Based on the physical model described in Sec. II, we study the transient charge responses of *M-F-M* and *M-F-I-M* capacitors, including hysteresis loops and pulse-switching dynamics. The underlying physics behind the recent experimental observations is discussed in detail. For convenience, the theoretical model is implemented in a circuit-compatible manner so that all the dynamic simulations can be performed accurately and self-consistently in the SPICE simulator. The detailed implementation can be found in Ref. [17].

A. *M-F-M* capacitors

The *M-F-I-M* stack structure of interest is $TiN/Hf_{0.5}Zr_{0.5}O_2/Al_2O_3/TiN$ capacitors, where Zr-doped hafnium oxides (HZO) are a widely used FE material in the recent experimental measurements [6,14–16,21]. Before we study the *M-F-I-M* capacitors, we first extract the FE parameters by simulating the hysteresis loops of TiN/HZO/TiN *M-F-M* capacitors based on the conventional polarization-voltage (*P-V*) measurements. As suggested by the experiments [33–36], an interfacial oxide layer is likely to form between the FE layer and the metal contacts during the fabrication process of *M-F-M* capacitors. In this regard, an ultrathin DE layer is introduced at the FE-metal interface of a *M-F-M* capacitor. Note that the depolarization, which is caused by the finite screening effect of the metal contacts, manifests itself with the interfacial oxide layer [37]. Based on the *P-V* measurement

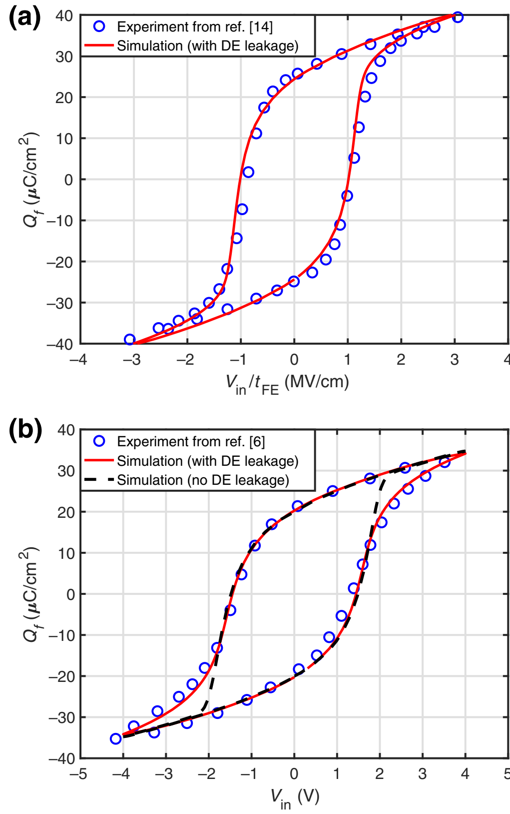

FIG. 2. (a) The simulated hysteresis loop of a TiN/11.3-nm HZO/TiN *M-F-M* capacitor in comparison with the experimental data extracted from Ref. [14]. (b) The simulated hysteresis loop of a TiN/10-nm HZO/TiN *M-F-M* capacitor in comparison with the experimental data extracted from Ref. [6]. The simulation without an interfacial oxide layer and the associated DE leakage is plotted for comparison.

in Ref. [14], the equivalent oxide thickness (EOT) of the interfacial oxide layer is found to be around 0.1 nm given that the dielectric constant of SiO_2 (ϵ_{SiO_2}) is 3.9. The corresponding interfacial capacitance $C_{DE} = \epsilon_0\epsilon_{SiO_2}/EOT \approx 0.35$ F/m^2, which is consistent with the reported value for the HZO/TiN interface [37]. The physical thickness of the interfacial oxide layer can be estimated to be 0.9 nm given the relative permittivity of 36 for the tetragonal and orthorhombic phase in HfO_2 and ZrO_2 [37]. Figure 2(a) shows the simulated hysteresis loop of a *M-F-M* capacitor based on the experimental *P-V* measurement in Ref. [14]. To further confirm the effect of an oxide layer between the FE and the metal contact, we simulate the hysteresis loop of a *M-F-M* capacitor from another measurement [6], as shown in Fig. 2(b). The simulation without considering the interfacial oxide layer is also plotted for comparison. Our simulations indicate that the oxide layer at the FE-metal interface may be one of the factors that could influence the hysteresis shape of *M-F-M*. The parameters extracted based on the experimental *P-V* measurement in Ref. [14] are summarized in Table I. The FE properties of 11.3-nm HZO are used for the study of *M-F-I-M* capacitors.

TABLE I. Parameters used for *M-F-M* from Ref. [14].

Parameter	Value
Area (A) (μm^2)	7000 [14]
FE thickness (t_{FE}) (nm)	11.3 [14]
α_1 (m/F)	-1.43×10^8
α_{11} (m^5 C^{-2}/F)	1.55×10^9
α_{111} (m^9 C^{-4}/F)	1.1×10^9
κ	10
L([Ω m]$^{-1}$)	3×10^{-3}
EOT (t_{DE}) (nm)	0.1
α (A/V^2)	9.57×10^{-16}
Frequency (kHz)	10 [14]
Pulse amplitude (V)	3.5 [14]

B. *M-F-I-M* capacitors

To study the TiN/HZO/AO/TiN capacitor, we apply the parameters obtained from the preceding section for 11.3-nm HZO. Based on the experimental setup in Ref. [14], ascending and descending pulse trains with a 600-ns pulse width (PW) are applied to the *M-F-I-M* capacitor with 11.3-nm HZO and 4-nm AO. One of the voltage pulses and the total current flowing through the external resistor are shown in Fig. 3(a). Figure 3(b) shows the corresponding transient free charge responses from the simulation. In the steady state before the pulse voltage is applied, the FE layer is in the negative remanent polarization (P_r) state, as suggested in Ref. [14]. To compensate the FE charge density, there must be the same amount of charges with opposite signs at the FE-DE interface. However, a dielectric material like AO cannot support a charge density as large as around 20 μC/cm^2 for such a long period of time without breakdown [31,32]. Therefore, here the initial DE charge $\widetilde{Q}_{DE}(0)$ is assumed to be 7 μC/cm^2 reported in Ref. [31], and the rest of the compensating charges are from the interfacial trapped charge Q_{it} [31]. Such a large amount of trapped charges are likely to be introduced through the DE leakage to the FE-DE interface during the wake-up process after the fabrication. At a large pulse amplitude, a large amount of negative DE charges accumulated at the FE-DE interface indicate that most of the applied voltage is across the DE layer in this stack system. Thus, in such pulse measurements, the FE polarization is barely switched even if a large voltage is applied. Similar to the experiments, the release charge Q_D is defined as the difference between the maximum charge Q_{max} and the residual charge Q_{res} at a given pulse amplitude V_a; that is, $Q_D = Q_{max} - Q_{res}$. At a fixed kinetic coefficient $L = 6 \times 10^{-3}(\Omega\text{m})^{-1}$, it is found that Q_D of *M-F-I-M* is enhanced without hysteresis compared to the measured charges on the associated standalone 4-nm AO capacitor,

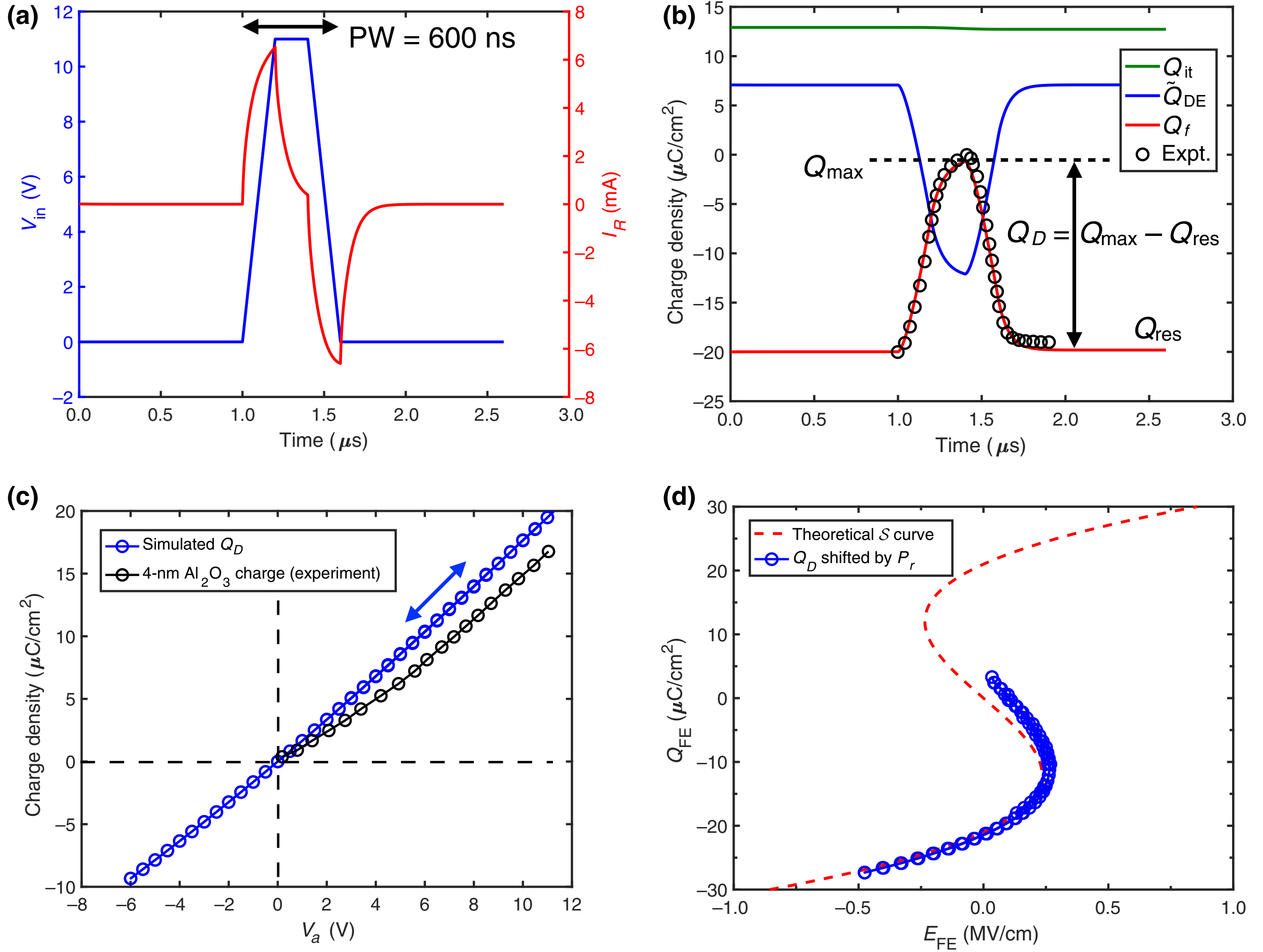

FIG. 3. (a) The applied pulse V_{in} from Ref. [14] (left) and the simulated current flowing through the series resistor I_R (right). (b) Simulated transient responses of the free charge Q_f and the calculated DE charge Q_{DE} and trapped charge Q_{it} in comparison with the measured free charge response extracted from Ref. [14]. The definitions of Q_{max}, Q_{res}, and Q_D in the main text are also shown. (c) The release charge Q_D at ascending and descending pulse trains with the amplitude V_a: 0 V → 12 V → −6 V → 0 V, showing the hysteresis-free charge boost compared to the charges on the associated AO capacitor extracted from Ref. [14]. (d) The simulated hysteresis-free S curve compared to the static curve predicted by the Landau formalism using the FE material parameters obtained in Sec. III A.

as shown in Fig. 3(c). From the simulation, the electric field across the FE oxide, $E_{FE} = V_{FE}/t_{FE}$, can be directly obtained, and the theoretical static curve is derived from Eq. (4) in the steady state:

$$E_{FE} = 2\alpha_1 P + 4\alpha_{11} P^3 + 6\alpha_{111} P^5. \quad (8)$$

Figure 3(d) shows that an S curve with negligible hysteresis can be achieved with the DE leakage parameter $\alpha = 2 \times 10^{-16}$ A/V^2. For the static curve, Q_D is shifted by P_r, which is the initial reference point and is reported as around 18 μC/cm^2 [14]. Note that the S curve obtained from the simulation does not go through the origin because L for the FE response is not calibrated dynamically based on the polarization charge responses.

In Fig. 4(a), we show that the experimentally observed charge boost is mainly determined by the kinetic coefficient L. The increasing L indicates the faster FE charge responses to the applied voltage, leading to larger maximum charges Q_{max} in the same PW. Hence, the release charge Q_D can be enhanced with less FE domain viscosity. To further confirm this finding, we also explore the effect of DE leakage α and find that the DE leakage is not a dominant factor in the observed charge-boost effect, as shown in Fig. 4(b).

Based on the experimentally measured free charge response from Ref. [14], the kinetic coefficient L can be numerically extracted at a given pulse amplitude. With extracted L, Fig. 5(a) demonstrates that the charge boost is enhanced when the applied pulse is large enough to induce

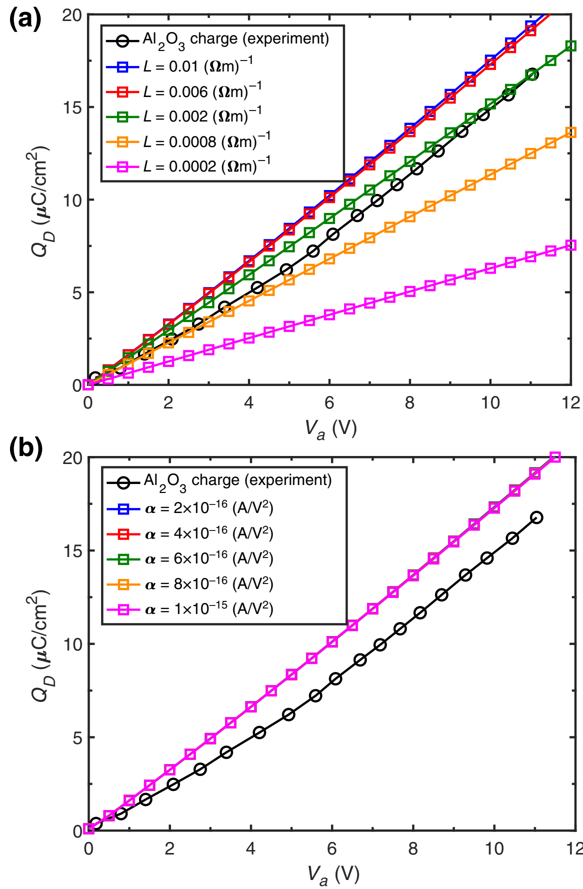

FIG. 4. (a) The effect of L on the charge-boost effect. As L increases, the release charge Q_D on M-F-I-M gradually becomes larger than that on the associated DE capacitor. (b) The effect of α on the charge boost, which indicates that the charge boost is not dominated by the DE leakage. The charges on AO are extracted from the measurements in Ref. [14].

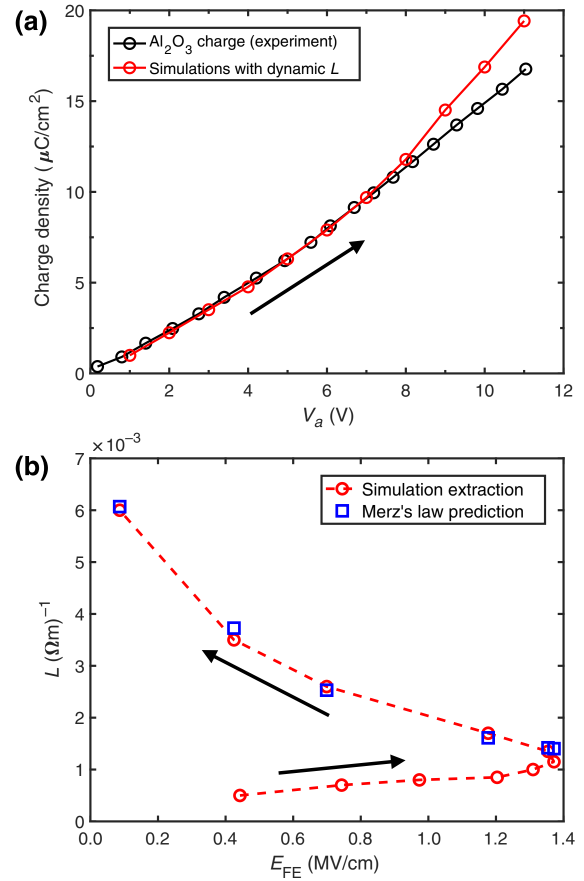

FIG. 5. (a) The corresponding Q_D using L extracted based on the charge responses in Ref. [14], where charges on AO are from Ref. [14] as well. (b) The extracted L in the NC region compared to the Merz's law prediction with $E_0 = 0.12$ MV/cm. The turning point of E_{FE} indicates the onset of NC region. The black arrows in (a),(b) indicate the applied voltage sweep direction.

the FE response, whereas a small applied pulse results only in the DE response in the FE layer and thus no charge boost is observed. As a reciprocal of the domain viscosity, L is assumed to be proportional to the domain-wall mobility μ_d corresponding to the domain nucleation; that is, $L \propto \mu_d$. Based on Merz's law [24], the relationship between L and nonzero E_{FE} can be derived:

$$L \propto \frac{\mu_d |E_{\mathrm{FE}}|}{|E_{\mathrm{FE}}|} \propto \frac{1}{|E_{\mathrm{FE}}|} v_d \propto \frac{1}{|E_{\mathrm{FE}}|}\frac{1}{t_s} \propto \frac{1}{|E_{\mathrm{FE}}|} e^{-E_0/|E_{\mathrm{FE}}|}, \tag{9}$$

where v_d is the domain-wall velocity inversely proportional to the switching characteristic time t_s, and E_0 is the activation field for domain switching [24]. Figure 5(b) shows that when the FE is driven into the NC region, L can be described by Merz's law, which suggests the domains are likely to be in the creep region as the electric field across the FE (E_{FE}) becomes smaller [38]. From Eq. (9), as $|E_{\mathrm{FE}}|$ approaches 0^+, L is asymptotic to zero because of zero driving force for domain switching. Before FE domain switching, only the DE response is induced, and L is found to be linearly dependent on E_{FE}.

In contrast to the TiN/11.3-nm HZO/4-nm AO/TiN capacitor, the charge hysteresis was observed in a TiN/11.3-nm HZO/1-nm AO/TiN capacitor [14]. It was suggested that the appearance of such hysteresis was attributed to the capacitance mismatch between the FE and the DE layer as the DE thickness decreases based on the theory of NC stabilization. However, here we demonstrate that such hysteresis is caused by the DE leakage and the associated interfacial trapped charge dynamics instead of NC stabilization. At the pulse trains with ascending and descending amplitudes, Figs. 6(a) and 6(b) show the charge responses of the 11.3-nm HZO/4-nm AO stack and the 11.3-nm HZO/1-nm AO stack, respectively. For the 11.3-nm HZO/4-nm AO stack, when a large voltage is across the DE layer, DE leakage is induced and therefore, the trapped charges leak out through the DE, as can

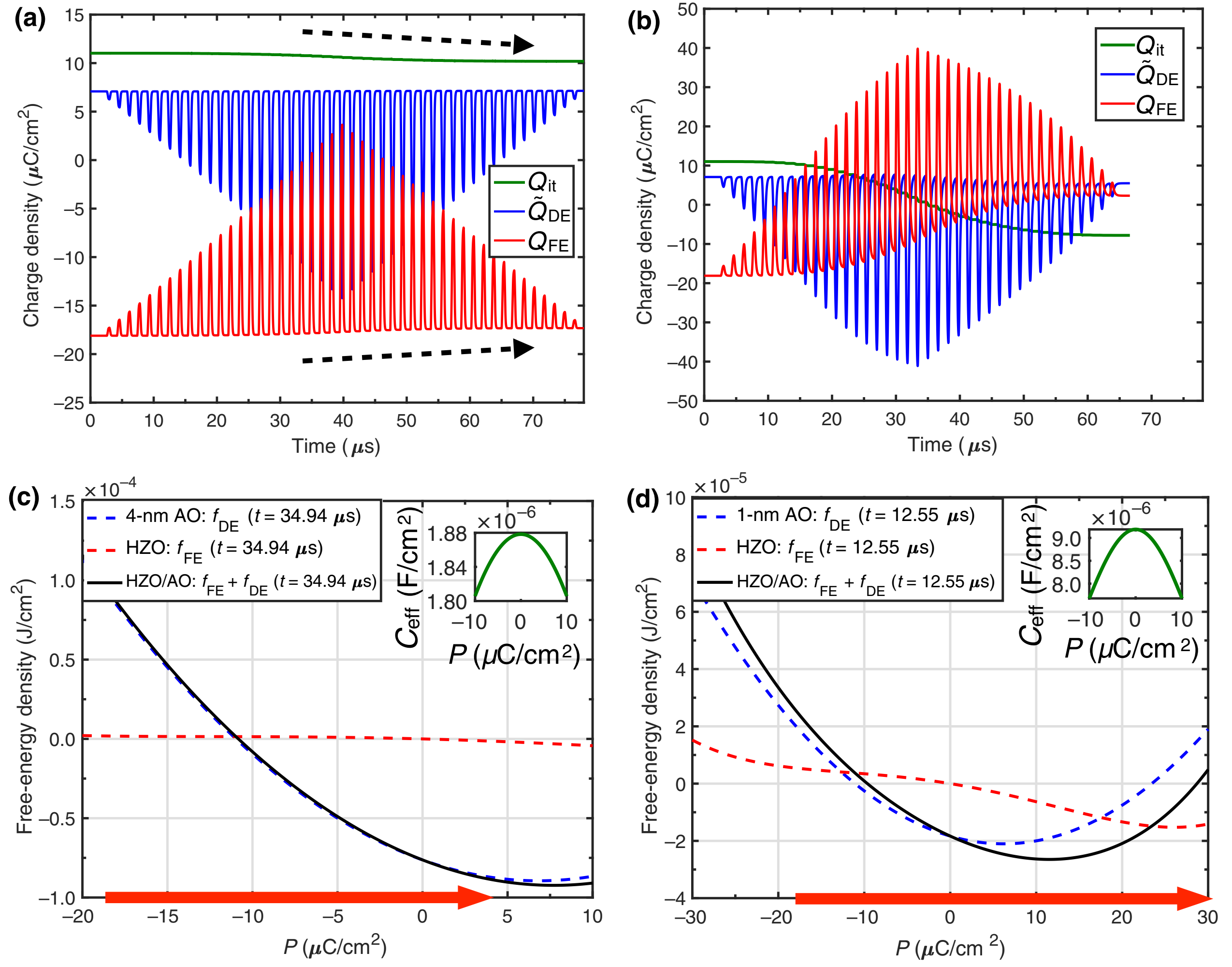

FIG. 6. (a) Charge responses of the 11.3-nm HZO/4-nm AO stack at ascending and descending pulse trains with the amplitude V_a: 0 V → 12 V → 0 V. The dashed arrows indicate the trapped charge leak and the increasing residual charges during the pulse trains. $\alpha = 2 \times 10^{-16}$ A/V^2 for the 4-nm AO stack. (b) Charge responses of the 11.3-nm HZO/4-nm AO stack at ascending and descending pulse trains with V_a: 0 V → 10 V → 0 V. $\alpha = 7.57 \times 10^{-16}$ A/V^2 for the 1-nm AO stack. (c) The free-energy profiles of the 11.3-nm HZO, the 4-nm AO, and the corresponding HZO/AO stack near zero polarization at $t = t_0$. The red arrow indicates the switching range of P during the simulation. (d) The free-energy profiles of the 11.3-nm HZO, the 1-nm AO, and the corresponding HZO/AO stack near zero polarization at $t = t_0$. The red arrow indicates the switching range of P during the simulation.

be seen from the slightly decreased Q_{it} in Fig. 6(a). As a result, the residual charges of Q_f after each pulse gradually increase in Fig. 6(a). For the 11.3-nm HZO/1-nm AO stack in Fig. 6(b), the leakage effect becomes more evident compared to the 11.3-nm HZO/4-nm AO stack. The simulations indicate that the possible cause of the increasing residual charges after pulse switching experimentally observed in Ref. [14], especially at a large pulse amplitude, can be explained by the transient responses of trapped charges at the FE-DE interface. Furthermore, from Figs. 6(a) and 6(b) and Eq. (6), one can infer that the role of the initial DE charge $\tilde{Q}_{DE}(0)$ plays in the transient responses is a shift in $\tilde{Q}_{DE}$ and Q_{it} dynamics, which means that the choice of the $\tilde{Q}_{DE}(0)$ value does not affect the conclusions drawn from the simulations.

The hysteresis behavior can be studied with the curvature of the total free-energy profile of the system near polarization reversal. The Landau free energy of the FE in a unit of J/m^2 is given by

$$f_{FE} = (\alpha_1 P^2 + \alpha_{11} P^4 + \alpha_{111} P^6 - E_{FE} P) t_{FE}. \quad (10)$$

The energy stored in a capacitor in terms of P can be derived as

$$\begin{aligned} f_{DE} &= Q_{DE}^2/(2C_{DE}) - Q_{DE} V_{DE} \\ &= (P - \Delta Q)^2/(2C_{DE}) - (P - \Delta Q) V_{DE}, \end{aligned} \quad (11)$$

where C_{DE} is the DE capacitance per unit area and $\Delta Q = P - Q_{DE}$ is the difference between polarization and the DE

charges, which is caused by the interfacial trapped charges. Figures 6(c) and 6(d) show the free-energy profiles of the FE, the DE, and the FE-DE stacks at $t = t_0$, where t_0 is the time at which P is around 0 μC/cm^2. Note that in the presence of the trapped charges, the FE and DE energy profiles do not align at $P = 0$ μC/cm^2 because the FE charges are not totally compensated by the DE charges. In the 11.3-nm HZO/4-nm AO stack, polarization P is switched between one of the energy minimums and the energy maximum, as indicated by the red arrow in Fig. 6(c). In other words, P does not go to the other energy minimum state. Note that when P is around the energy maximum, the FE is driven into its NC region, where the curvature of the free-energy profile (and the FE capacitance) is negative. The effective capacitance C_{eff} of the M-F-I-M system can be obtained by calculating the curvature of the total free-energy profile:

$$C_{\text{eff}} = \left(\frac{\partial^2 f_{\text{DE}}}{\partial P^2} + \frac{\partial^2 f_{\text{FE}}}{\partial P^2}\right)^{-1}. \tag{12}$$

From Eq. (12), C_{eff} is positive when the positive DE capacitance is dominant over the negative FE capacitance. With a positive C_{eff}, the NC region gets stabilized and no hysteresis is expected according to the NC theory [3,39]. Note that ΔQ in Eq. (11) (and thus trapped charges) does not affect the effective capacitance.

As shown in the inset of Fig. 6(c), the effective capacitance of the 4-nm AO stack is positive around zero polarization, indicating the FE-DE capacitance match and thus hysteresis-free NC stabilization. For the 1-nm AO stack, the effective capacitance is also positive around zero polarization, as shown in the inset of Fig. 6(d). Therefore, based on the theory of NC stabilization, such a 1-nm AO stack is not expected to show hysteresis. However, consistent with the experimental findings in Ref. [14], the release charge Q_D of such a 1-nm AO stack shows clear hysteresis with the DE leakage parameter $\alpha = 7.57 \times 10^{-16}$ A/V^2 in the simulation, as shown in Fig. 7. Note that α of the 1-nm AO stack is larger than that of the 4-nm AO stack due to the larger leakage current in a thinner DE. In contrast to the 4-nm AO stack, the FE polarization of the 1-nm AO stack is driven into the other energy minimum state in the measurement, as indicated by the red arrow in Fig. 6(d). The appearance of hysteresis in the 1-nm AO stack can be attributed to the increasing FE charge responses due to the larger DE leakage of the thinner DE compared to the 4-nm AO stack. Therefore, we show that the hysteresis observed in a M-F-I-M stack with a reduced DE thickness is caused not by the FE-DE capacitance mismatch but by the fact that the FE polarization transitions from one state to the other state with the help of DE leakage. This finding is consistent with the previous experimental observation of FE-gated Ge p-channel transistors [40]. In addition, Fig. 7 shows that, for the M-F-I-M with 1-nm AO, the maximum release charge difference in the hysteresis $\Delta Q_D \approx 5.2$ μC/cm^2 at

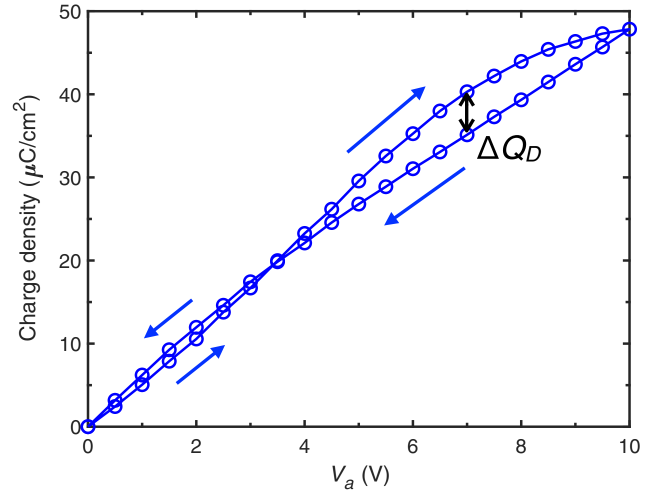

FIG. 7. The release charge Q_D of the 11.3-nm HZO/1-nm AO stack with $\alpha = 7.57 \times 10^{-16}$ A/V^2 shows clear hysteresis in a clockwise manner, as observed in Ref. [14].

the pulse amplitude of 7 V, which is close to the reported value of 4.7 μC/cm^2 in Ref. [14]. Note that the hysteresis direction is in a clockwise manner, which is also consistent with the experimental measurements in Ref. [14].

As a final remark, although we demonstrate the dynamics of trapped charges in response to the pulse measurements in this work, the frequency and temperature responses of the FE polarization and the corresponding trapped charges may rely on a better understanding of microscopic behaviors of HfO_2-based FE [41]. In addition, the interplay between the trapped charge dynamics and FE polarization switching also requires more experimental characterization, especially for nonvolatile memory applications [6,42].

IV. CONCLUSION

In summary, this paper presents underlying physical mechanisms for the hysteresis-free negative capacitance effect experimentally observed in M-F-I-M capacitors. With the DE leakage and interfacial trapped charges included, we extract the FE parameters by capturing the measured hysteresis loops of M-F-M capacitors. Significantly, for M-F-I-M stacks, we show (i) the charge boost is mainly determined by the faster FE domain responses near the polarization reversal and (ii) the charge responses would show hysteresis as long as the FE polarization is switched from one state to the other with the aid of DE leakage. The analyses of thermodynamic energy profiles in the presence of interfacial trapped charges indicate that the observed hysteresis in M-F-I-M is caused by the FE polarization switching rather than the FE-DE capacitance mismatch suggested by the theory of NC stabilization. The theoretical demonstrations provide useful physical insights

into the alleged static NC effect for emerging low-power logic devices.

ACKNOWLEDGMENTS

This work is funded by Intel Corporation through Semiconductor Research Corporation MSR-INTEL TASK 2835.001.

[1] G. E. Moore, Cramming more components onto integrated circuits, Proc. IEEE **86**, 82 (1998).

[2] Nam Sung Kim, T. Austin, D. Blaauw, T. Mudge, K. Flautner, Jie S. Hu, M. J. Irwin, M. Kandemir, and V. Narayanan, Leakage current: Moore's law meets static power, Computer **36**, 68 (2003).

[3] Sayeef Salahuddin and Supriyo Datta, Use of negative capacitance to provide voltage amplification for low power nanoscale devices, Nano Lett. **8**, 405 (2008).

[4] Sou-Chi Chang, Uygar E. Avci, Dmitri E. Nikonov, and Ian A. Young, A thermodynamic perspective of negative-capacitance field-effect transistors, IEEE J. Exploratory Solid-State Comput. Devices Circuits **3**, 56 (2017).

[5] Chia-Sheng Hsu, Chenyun Pan, and Azad Naeemi, Performance analysis and enhancement of negative capacitance logic devices based on internally resistive ferroelectrics, IEEE Electron Device Lett. **39**, 765 (2018).

[6] Kai Ni, Pankaj Sharma, Jianchi Zhang, Matthew Jerry, Jeffery A. Smith, Kandabara Tapily, Robert Clark, Souvik Mahapatra, and Suman Datta, Critical role of interlayer in $Hf_{0.5}Zr_{0.5}O_2$ ferroelectric FET nonvolatile memory performance, IEEE Trans. Electron Devices **65**, 2461 (2018).

[7] Kai Ni, Matthew Jerry, Jeffrey A. Smith, and Suman Datta, in *2018 IEEE Symposium on VLSI Technology* (IEEE, Honolulu, HI, 2018).

[8] Asif Islam Khan, Korok Chatterjee, Brian Wang, Steven Drapcho, Long You, Claudy Serrao, Saidur Rahman Bakaul, Ramamoorthy Ramesh, and Sayeef Salahuddin, Negative capacitance in a ferroelectric capacitor, Nat. Mater. **14**, 182 (2015).

[9] Weiwei Gao, Asif Khan, Xavi Marti, Chris Nelson, Claudy Serrao, Jayakanth Ravichandran, Ramamoorthy Ramesh, and Sayeef Salahuddin, Room-temperature negative capacitance in a ferroelectric–dielectric superlattice heterostructure, Nano Lett. **14**, 5814 (2014).

[10] Daniel J. R. Appleby, Nikhil K. Ponon, Kelvin S. K. Kwa, Bin Zou, Peter K. Petrov, Tianle Wang, Neil M. Alford, and Anthony O'Neill, Experimental observation of negative capacitance in ferroelectrics at room temperature, Nano Lett. **14**, 3864 (2014).

[11] Yu Jin Kim, Hiroyuki Yamada, Taehwan Moon, Young Jae Kwon, Cheol Hyun An, Han Joon Kim, Keum Do Kim, Young Hwan Lee, Seung Dam Hyun, Min Hyuk Park, and Cheol Seong Hwang, Time-dependent negative capacitance effects in $Al_2O_3/BaTiO_3$ bilayers, Nano Lett. **16**, 4375 (2016).

[12] Michael Hoffmann, Milan Pešić, Korok Chatterjee, Asif I. Khan, Sayeef Salahuddin, Stefan Slesazeck, Uwe Schroeder, and Thomas Mikolajick, Direct observation of negative capacitance in polycrystalline ferroelectric HfO_2, Adv. Funct. Mater. **26**, 8643 (2016).

[13] Sou-Chi Chang, Uygar E. Avci, Dmitri E. Nikonov, Sasikanth Manipatruni, and Ian A. Young, Physical Origin of Transient Negative Capacitance in a Ferroelectric Capacitor, Phys. Rev. Appl. **9**, 014010 (2018).

[14] M. Hoffmann, B. Max, T. Mittmann, U. Schroeder, S. Slesazeck, and T. Mikolajick, in *2018 IEEE International Electron Devices Meeting (IEDM)* (IEEE, San Francisco, CA, 2018).

[15] Michael Hoffmann, Franz P. G. Fengler, Melanie Herzig, Terence Mittmann, Benjamin Max, Uwe Schroeder, Raluca Negrea, Pintilie Lucian, Stefan Slesazeck, and Thomas Mikolajick, Unveiling the double-well energy landscape in a ferroelectric layer, Nature **565**, 464 (2019).

[16] Keum Do Kim, Yu Jin Kim, Min Hyuk Park, Hyeon Woo Park, Young Jae Kwon, Yong Bin Lee, Han Joon Kim, Taehwan Moon, Young Hwan Lee, Seung Dam Hyun, Baek Su Kim, and Cheol Seong Hwang, Transient negative capacitance effect in atomic-layer-deposited $Al_2O_3/Hf_{0.3}Zr_{0.7}O_2$ bilayer thin film, Adv. Funct. Mater. **29**, 1808228 (2019).

[17] Chia-Sheng Hsu, Sou-Chi Chang, Dmitri E. Nikonov, Ian A. Young, and Azad Naeemi, A theoretical study of multidomain ferroelectric switching dynamics with a physics-based SPICE circuit model for phase-field simulations, IEEE Trans. Electron Devices **67**, 2952 (2020).

[18] T. S. Böscke, J. Müller, D. Bräuhaus, U. Schröder, and U. Böttger, Ferroelectricity in hafnium oxide thin films, Appl. Phys. Lett. **99**, 102903 (2011).

[19] Johannes Müller, Tim S. Böscke, Uwe Schröder, Stefan Mueller, Dennis Bräuhaus, Ulrich Böttger, Lothar Frey, and Thomas Mikolajick, Ferroelectricity in simple binary ZrO_2 and HfO_2, Nano Lett. **12**, 4318 (2012).

[20] P. Sharma, K. Tapily, A. K. Saha, J. Zhang, A. Shaughnessy, A. Aziz, G. L. Snider, S. Gupta, R. D. Clark, and S. Datta, in *2017 Symposium on VLSI Technology* (IEEE, Kyoto, Japan, 2017).

[21] Masaharu Kobayashi, Nozomu Ueyama, Kyungmin Jang, and Toshiro Hiramoto, *2016 IEEE International Electron Devices Meeting (IEDM)* (IEEE, San Francisco, CA, 2016).

[22] Muhammad A. Alam, Mengwei Si, and Peide D. Ye, A critical review of recent progress on negative capacitance field-effect transistors, Appl. Phys. Lett. **114**, 090401 (2019).

[23] Zhan Liu, Hao Jiang, Brandon Ordway, and T. P. Ma, Unveiling the apparent "negative capacitance" effects resulting from pulse measurements of ferroelectric-dielectric bilayer capacitors, IEEE Electron Device Lett. **41**, 1492 (2020).

[24] Walter J. Merz, Switching time in ferroelectric $BaTiO_3$ and its dependence on crystal thickness, J. Appl. Phys. **27**, 938 (1956).

[25] Alexander K. Tagantsev, Landau expansion for ferroelectrics: Which variable to use?, Ferroelectrics **375**, 19 (2008).

[26] L. D. Landau, On the theory of phase transitions, Zh. Eksp. Teor. Fiz **7**, 19 (1937).

[27] V. L. Ginzburg, On the dielectric properties of ferroelectric (segnette-electric) crystals and barium titanate, Zh. Eksp. Teor. Fiz **15**, 739 (1945).

[28] A. F. Devonshire, XCVI. Theory of barium titanate: Part I, London, Edinburgh, Dublin Philos. Mag. J. Sci. **40**, 1040 (1949).

[29] Maya D. Glinchuk, Anna N. Morozovska, Anna Lukowiak, Wieslaw Strek, Maxim V. Silibin, Dmitry V. Karpinsky, Yunseok Kim, and Sergei V. Kalinin, Possible electrochemical origin of ferroelectricity in HfO_2 thin films, J. Alloys Compd. **830**, 153628 (2020).

[30] X. Lyu, M. Si, X. Sun, M. A. Capano, H. Wang, and P. D. Ye, in *2019 Symposium on VLSI Technology* (IEEE, Kyoto, Japan, 2019).

[31] Mengwei Si, and Xiao Lyu, and Peide D. Ye, Ferroelectric polarization switching of hafnium zirconium oxide in a ferroelectric/dielectric stack, ACS Appl. Electron. Mater. **1**, 745 (2019).

[32] H. C. Lin, P. D. Ye, and G. D. Wilk, Leakage current and breakdown electric-field studies on ultrathin atomic-layer-deposited Al_2O_3 on GaAs, Appl. Phys. Lett. **87**, 182904 (2005).

[33] Milan Pešić, Franz Paul Gustav Fengler, Luca Larcher, Andrea Padovani, Tony Schenk, Everett D. Grimley, Xiahan Sang, James M. LeBeau, Stefan Slesazeck, Uwe Schroeder, and Thomas Mikolajick, Physical mechanisms behind the field-cycling behavior of HfO_2-based ferroelectric capacitors, Adv. Funct. Mater. **26**, 4601 (2016).

[34] Han Joon Kim, Min Hyuk Park, Yu Jin Kim, Young Hwan Lee, Taehwan Moon, Keum Do Kim, Seung Dam Hyun, and Cheol Seong Hwang, A study on the wake-up effect of ferroelectric $Hf_{0.5}Zr_{0.5}O_2$ films by pulse-switching measurement, Nanoscale **8**, 1383 (2016).

[35] Anastasia Chouprik, Maxim Spiridonov, Sergei Zarubin, Roman Kirtaev, Vitalii Mikheev, Yury Lebedinskii, Sergey Zakharchenko, and Dmitrii Negrov, Wake-up in a $Hf_{0.5}Zr_{0.5}O_2$ film: A cycle-by-cycle emergence of the remnant polarization via the domain depinning and the vanishing of the anomalous polarization switching, ACS Appl. Electron. Mater. **1**, 275 (2019).

[36] Youngin Goh, Sung Hyun Cho, Sang-Hee Ko Park, and Sanghun Jeon, Oxygen vacancy control as a strategy to achieve highly reliable hafnia ferroelectrics using oxide electrode, Nanoscale **12**, 9024 (2020).

[37] Patrick D. Lomenzo, Claudia Richter, Thomas Mikolajick, and Uwe Schroeder, Depolarization as driving force in antiferroelectric hafnia and ferroelectric wake-up, ACS Appl. Electron. Mater. **2**, 1583 (2020).

[38] J. Y. Jo, S. M. Yang, T. H. Kim, H. N. Lee, J.-G. Yoon, S. Park, Y. Jo, M. H. Jung, and T. W. Noh, Nonlinear Dynamics of Domain-Wall Propagation in Epitaxial Ferroelectric Thin Films, Phys. Rev. Lett. **102**, 045701 (2009).

[39] Asif Islam Khan, Ujwal Radhakrishna, Korok Chatterjee, Sayeef Salahuddin, and Dimitri A. Antoniadis, Negative capacitance behavior in a leaky ferroelectric, IEEE Trans. Electron Devices **63**, 4416 (2016).

[40] Jiuren Zhou, Genquan Han, Nuo Xu, Jing Li, Yue Peng, Yan Liu, Jincheng Zhang, Qing-Qing Sun, David Wei Zhang, and Yue Hao, Incomplete dipoles flipping produced near hysteresis-free negative capacitance transistors, IEEE Electron Device Lett. **40**, 329 (2019).

[41] Junkang Li, Yiming Qu, Mengwei Si, Xiao Lyu, and Peide D. Ye, in *2020 IEEE Symposium on VLSI Technology* (IEEE, Kyoto, Japan, 2020).

[42] K. Toprasertpong, M. Takenaka, and S. Takagi, in *2019 IEEE International Electron Devices Meeting (IEDM)* (IEEE, San Francisco, CA, 2019).